INVESTIGATION OF MICROSTRUCTURE, MECHANICAL PROPERTIES AND CORROSION BEHAVIOUR OF AS-CAST Mg-4Sn-2Al-X (X = 0.5 Ca AND 0.25 Mn) ALLOYS

Penbe Kurt
Biomedical Device Technology Program, Gedik Vocational School, Istanbul Gedik University, 34913 Istanbul, Turkey

S. Can Kurnaz
Engineering Faculty, Department of Metallurgical and Materials Engineering, Esentepe Campus, Sakarya University, 54187 Serdivan, Sakarya, Turkey

https://doi.org/10.1007/s40962-025-01576-w

Abstract

In this study, 0.5 wt. % of Ca, and 0.25 wt. % Mn was added to Mg-4Sn-2Al alloy, and its mechanical and corrosion properties were investigated. Production was carried out by gravity casting under a controlled atmosphere. Microstructures were investigated using SEM/EDS and XRD. In addition to the microstructure, the effects of alloying element addition on tensile properties, hardness, fracture surfaces, strain hardening exponent, anisotropy coefficients, corrosion microstructures, and corrosion rates were also investigated. According to the results obtained, Mg–4Sn–2Al–0.5Ca, and Mg–4Sn–2Al–0.25Mn alloys showed lower mechanical properties than Mg–4Sn–2Al alloys. While the ultimate tensile strength was 131 MPa for the Mg-4Sn-2Al alloy, this value decreased to 92.5 MPa with the addition of Ca, and to 102 MPa for the Mg-4Sn-2Al–0.25Mn alloy. Also, the strain hardening coefficient for Mg-4Sn-2Al alloy was 0.35, while it decreased to 0.28 with the addition of Ca. With the addition of Mn, it gave a value of 0.36, which is almost the same as Mg-4Sn-2Al alloy. When the anisotropy coefficients are examined, the anisotropy coefficient of Mg-4Sn-2Al alloy, which was 0.83, increased to 0.872 with the addition of Ca, and 1.293 with the addition of Mn. According to the results obtained from potentiodynamic and immersion corrosion tests, the Mn doped alloy showed the highest corrosion resistance in both tests. The corrosion rate of the Mn doped alloy was 18.96 mpy according to potentiodynamic results and 65.32 mpy according to immersion test results.

Keywords: *magnesium alloys, corrosion rate, casting, microstructure, mechanical properties, anisotropy*

Introduction

Magnesium (Mg), which has a closed-pack hexagonal (hcp) crystal structure, high specific strength, and low density is one of the lightest building materials widely used in areas such as automotive, biomedical, and aerospace.[1–6] The fact that it is the 8th most abundant element on earth, and is a 100% recyclable metal increases the interest in magnesium. However, some issues such as low corrosion resistance, low ductility, and hardness limit its use. These properties need to be improved for magnesium to compete with other metals in the light engineering metals market.

Alloying is one of the most used methods to improve the mechanical and corrosion properties of Mg. Choosing aluminum (Al), and tin (Sn) as alloying elements lowers the melting point of magnesium, and improves its ability to be cast, while still preserving its strength.[7,8]

Among the magnesium alloys, those based on the magnesium-aluminum (Mg-Al) system have an excellent combination of good castability, good corrosion resistance, acceptable room-temperature mechanical properties, and cost-effectiveness.[9,10] The addition of a particularly high Al content (more than 5%) increases the solubility of aluminum in the structure, and contributes to the mechanical properties due to solid solution hardening. The mechanical properties of these materials are negatively affected due to

Received: 30 October 2024 / Accepted: 13 February 2025 / Published online: 15 March 2025

the formation of $Mg_{17}Al_{12}$ precipitates at grain boundaries, and dendritic regions at high temperatures. The melting point of these precipitates is approximately 437 °C.[9,11–13] The low melting temperature of the $Mg_{17}Al_{12}$ phase causes deterioration of creep properties at temperatures above 125°C.[9,14] For these reasons, in this study, it was thought that it would be appropriate to add 2 wt. % Al to the alloys, especially to facilitate casting, and prevent the formation of the $Mg_{17}Al_{12}$ intermetallic phase.

Recently, researchers' interest in magnesium-tin (Mg-Sn) alloys has increased because of their potentially high performance at high temperature, and room temperature, and their low cost. Mg-Sn alloys, which have great potential in terms of creep resistance, are of particular interest. The Mg_2Sn phase (melting temperature approximately 770°C) is thermally stable. During the casting process, this phase is distributed along the grain boundaries.[9,15] The Mg_2Sn phase can be easily precipitated due to the high solubility limit of Sn in Mg at 561 °C (14.85%), and its low solubility at room temperature.[16] These two factors contribute to the improvement of strength properties at ambient conditions, and high temperatures.[9,17] In the study conducted by Park et al. in 2009, 1%, 5%, and 9% Sn were added to the cast Mg-5Al-1Zn alloy, and its corrosion properties were examined in 3.5% NaCl solution.[18] It was stated that adding 5% Sn increased the corrosion resistance of the alloy. Mg-5Al-1Zn alloy mainly consists of α-Mg, and $Mg_{17}Al_{12}$ phases. As the amount of wt. % Sn increased, the volume of the Mg_2Sn phase also increased and a coarsening trend was observed. As a result, the semi-continuous microstructure with the addition of Sn caused the corrosion rate to decrease. However, when the Sn ratio was 9 wt%, the volume fractions of Mg_2Sn and $Mg_{17}Al_{12}$ phases increased further. The Mg_2Sn and $Mg_{17}Al_{12}$ phases in the structure increased the number of galvanic cells formed, causing the corrosion resistance to decrease. In another study, it was stated that adding 0.5 wt. % Sn to AZ91 alloy increased tensile strength and elongation, and also improved fluidity.[19] In 2015, it was stated that the strength of the alloy increased gradually with tin additions between 2%, and 6 wt% of the Mg-8Al-2Zn alloy.[20] As the amount of Sn added increased, the size of the recrystallized grains decreased gradually. Also, the amount of fine Mg_2Sn precipitates increased, leading to better yield strength. In addition to the application of Sn as the main alloying element, elements such as Al, Ca, and Mn are chosen as alloying elements for their effects on the formation of intermetallic phases to improve mechanical properties at room temperature, and high temperatures.[21] Moreover, in the study of Liu et al. in 2007, it was stated that the mechanical properties were improved with the addition of (1-10%) Sn to Magnesium.[22] It has been shown that alloys with (4-6%) Sn content give the best results. Therefore, in this study, the Sn ratio was determined as 4% in order not to increase the density of the alloy, and the size of Mg_2Sn intermetallics excessively.

The alkaline earth element calcium (Ca) is a preferred alloying element due to its positive properties such as a low melting point of 842 °C, a low density of 1.55 $gr.cm^{-3}$ (similar to Mg), and low cost. While magnesium is flammable, calcium has flame-retardant properties. It has also been reported that the addition of Ca to Mg alloys has a positive effect on grain refinement.[23,24] Bao et al. reported that adding Ca to Mg-Sn alloys induces structural changes in the secondary phase.[25] Similarly, a study conducted by Suresh at al. emphasized that the Sn/Ca ratio is a critical parameter in Mg-Sn-Ca alloys, determining the types of phases formed.[26] According to Nayyeri and Mahmudi, adding Ca to Mg-Sn alloys leads to the formation of the Mg_2Sn phase at grain boundaries, along with a needle-like CaMgSn ternary phase observed both in the matrix, and at grain boundaries.[27] Furthermore, it has been highlighted that the size and composition of the phases in the microstructure significantly influence the corrosion behavior and mechanical properties of Mg alloys. Additionally, the grain refinement achieved through Ca addition has been found to play a key role in altering the mechanical and corrosion properties of Mg-Sn-Ca alloys. In the study conducted by Hua et al., the effects of equal additions of Sn, and Ca (0.3:0.1, 0.6:0.2, 1.2:0.4, wt %) on the microstructure, mechanical properties, and corrosion behavior of Mg-Sn-Ca-based alloys were investigated.[28] With the addition of 0.4 Ca, the grain size decreased, and accordingly, the UTS and YTS values increased. According to the corrosion test results, the highest corrosion resistance was obtained in the alloy with 0.4 Ca addition. According to the findings of Song et al., calcium content lower than 0.7 wt% effectively reduces corrosion.[29]

Table 1. Chemical Composition of Alloys

Alloy No.	Alloy	Actual compositions (wt. %)				
		Sn	Al	Ca	Mn	Mg
1	Mg-4Sn-2Al	4.4	1.79	–	–	Bal.
2	Mg-4Sn-2Al-0.5Ca	4.3	1.42	0.53	–	Bal.
3	Mg-4Sn-2Al-0.25Mn	4.4	1.48	–	0.25	Bal.

Figure 1. Schematic illustration of the casting process.

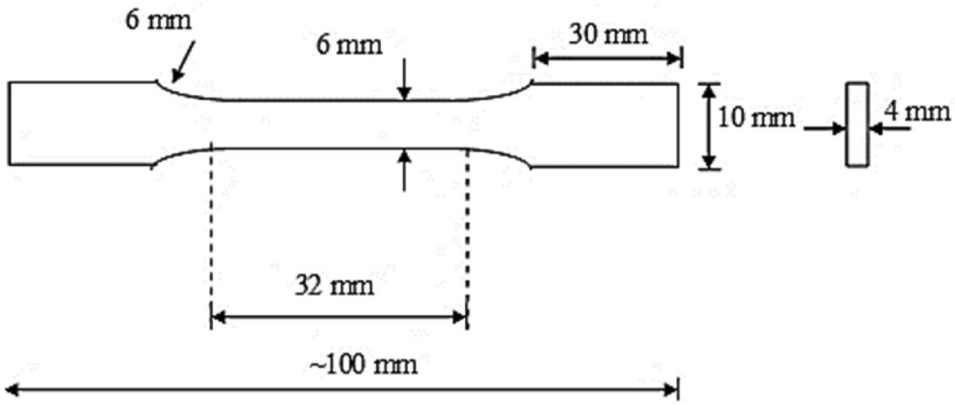

Figure 2. Shape and size of tensile specimens.

Manganese (Mn), which can reduce the corrosion rate, and increase the strength of Mg alloys, is a widely used alloying element option in industry. Due to its low solubility in magnesium, it can slowly diffuse into the matrix, and precipitate into fine particles.[30–32] In addition, when preparing Mg-Al-Zn alloys, the alloying element Mn is usually added to Mg-Al alloys to improve mechanical properties. Adding aluminum, and zinc to magnesium increases strength and castability, while manganese is added to increase ductility. Aravindan et al. selected the Mn content as 0.4 wt. % for AZ91D alloy.[33] The researchers discovered that when Mn was added to Mg alloys at less than 0.6 wt.%, the grains became smaller, reducing the amount of Fe impurities, and leading to a lower corrosion rate. Also recently, it has been shown that Al will preferentially combine with Mn to form Al-Mn phases with high eutectic temperatures, and these phases may play an important role in high-temperature performance.[34] Moreover, manganese has a grain-refining effect. This feature accelerates the formation of a protective layer on the surface of the material, and increases the number of active atoms. Consequently, it enhances corrosion resistance by preventing the cathodic hydrogen evolution reaction.[35] In addition, low levels of Mn do not have a toxic effect and play a significant role in the activation of multiple enzyme systems.[36]

In a previous study, the addition of 2 wt. % La and 0.15 wt. % Ti to Mg-4Sn-2Al alloy was found to improve its mechanical, and corrosion properties.[37] It is curious how the addition of Ca, and Mn alloying elements to the same alloy will affect the results. In addition, due to their low density, magnesium alloys are preferred to meet the need for lightweight materials in many areas such as aerospace, automotive, and biomedical.[1–3] This study is important because of the potential of adding low amounts of Ca, and Mn to Mg alloys to expand their usability in applications by improving their mechanical properties, and corrosion resistance without compromising their lightness. The primary reason for selecting 0.5 wt. % of Ca, and 0.25 wt. % Mn in Mg alloys is to achieve optimal effects on microstructure, mechanical properties, and corrosion

behavior. This concentration promotes grain refinement, leading to a more homogeneous microstructure while preventing the formation of undesirable large intermetallic phases. Additionally, Mn contributes to reducing corrosion by forming a protective surface film, while Ca enhances corrosion resistance and minimizes the risk of galvanic coupling at low levels. From a mechanical perspective, this composition provides an ideal balance between strength and ductility, supports solid solution strengthening, and prevents alloy brittleness. Moreover, it offers favorable casting fluidity, and machinability characteristics. Studies in the literature also demonstrate that a 0.5 wt.% Ca, and 0.25 wt. % Mn concentration often yields positive outcomes. Economically, this concentration provides effective improvements without significantly increasing the alloy's cost, making it a practical, and efficient choice.

Experimental Approach

The alloys, whose chemical compositions are given in Table 1, were prepared by gravity casting in an electric furnace, and steel crucibles using high-purity Mg, Sn, Al, Ca, and Mg-5Mn. The casting process was carried out with 1 kg of each alloy. The mold temperature was chosen as 100 °C, and the casting temperature was 750 °C, which is a commonly used temperature in the literature.[14,37] A gas mixture of CO_2-2% SF_6 (carbon dioxide-sulfur hexafluoride) with a flow rate of 1.4 L/min was used to prevent oxidation. The molten metal was poured into steel molds measuring 120x ϕ 110 mm in sealed cans filled with protective gas for 1 minute. The casting scheme is given in Figure 1. The chemical composition of the alloys shown in Table 1 was determined by the ICP-OES technique (Inductively coupled plasma-optical emission spectrometry).

The samples were prepared for metallography by cutting them using a wire erosion machine. Grinding was performed using silicon carbide (SiC) abrasive paper up to 1200 grit. A 1μm alumina solution was used to polish the samples. After polishing, the samples were cleaned with ethanol, and then dried. A solution consisting of picric acid, distilled water, acetic acid, and ethanol (4.5 g picric acid, 30 ml distilled water, 15 ml acetic acid, and 75 ml ethanol) was used for etching. Alloys were immersed in etchant for 5 seconds. After the etching process, the samples were washed with water, cleaned with ethanol, and dried with a hot air device. An X-ray diffractometer (Rigaku D-Max 2200) was used to determine the phases in the alloys, while a SEM instrument (JEOL 6060LV) with EDS was used to determine the distribution of elements in the samples.

The Brinell hardness measurement method was used for hardness measurements. Measurements were made with the Struers Duramin-500 device, and the ball diameter, and the load were chosen as 2.5 mm and 31.25 kg, respectively. Five readings were made, and the average of these values was accepted as the hardness value.

Tensile tests were measured at room temperature with an Instron 3367 universal tester at a 2 mm/min tensile speed. Tensile tests were performed using samples of ASTM E8M-21 (Figure 2) processed on the Wire Erosion device. Five measurements were made for each alloy, and averaged. A mechanical extensometer was used to determine the elongation.

The strain hardening exponent (n) was determined using data from tensile tests and Hollomon's equation (Equation 1) (ε is the actual strain, σ is the actual stress, and K is the strength coefficient, which is equal to the actual stress when the strain is 1.0). The anisotropy coefficient (r) is an essential factor in determining a metal's resistance to thinning at room temperature, and its formability. Permanent changes in thickness and length were measured with an extensometer during tensile tests, and the anisotropy coefficient (r) was calculated using Equation 2.[37]

$$\sigma = K\varepsilon^n \qquad \text{Eqn. 1}$$

$$r = \frac{\varepsilon_w}{\varepsilon_t} = \frac{\varepsilon_w}{-(\varepsilon_l + \varepsilon_w)} \qquad \text{Eqn. 2}$$

Corrosion tests were carried out in two ways: electrochemical, and immersion. Electrochemical corrosion tests were performed according to ASTM G59-97 standard.[38] Electrochemical measurements were performed using Gamry 300 electrochemical analyzer devices. Electrochemical, and immersion corrosion tests were performed in a 3.5% NaCl solution with a pH value of approximately 6. Only a surface area of 1.77 cm^2 was exposed to the solution. All potentiodynamic polarization experiments were conducted at room temperature (25°C), with a scanning rate of 1 mV/s within the range of -0.6 to +0.6V. Data were evaluated using the Gamry EChem Analyst software program. Equation 3 was used to determine the corrosion rate.[38]

$$R_{corr} = \frac{I_{corr}.K.EW}{d.A} \qquad \text{Eqn. 3}$$

In Equation 3, R_{corr} is the corrosion rate in mpy, EW is the equivalent weight in grams/equivalent, K is the constant (0.1288 $mpy.g.\mu A^{-1}.cm^{-1}$.), I_{corr} is the corrosion current in μA, d is the density in $grams.cm^{-3}$, A is the sample area in cm^2.

The immersion test was carried out on samples with a length of 35 mm, a width of 20 mm and a thickness of 4 mm, according to the G31-72(R-1999) standard.[39] The prepared samples were kept in % 3.5 NaCl solution with pH 6 at 25 °C for 120 hours, with the solution renewed every day. After the test, the corroded samples were

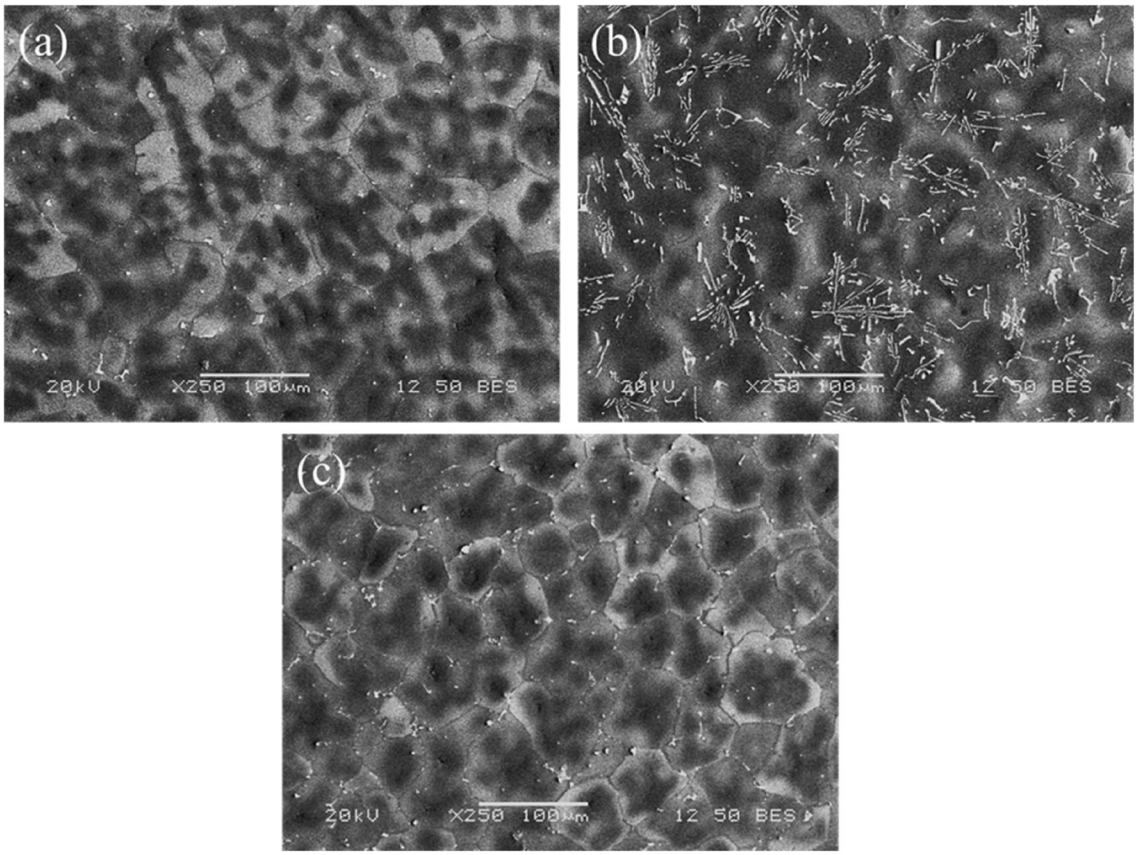

Figure 3. General microstructure SEM images of alloys (a) Alloy 1, (b) Alloy 2, and (c) Alloy 3.

cleaned using ethanol, weight loss was measured, and corrosion rates (R_w) were calculated according to Equation 4.[40]

$$R_w = \frac{K.W}{A.t.d} \qquad \text{Eqn. 4}$$

In Equation 4, K ($3.45x10^6$) is a constant in mpy, W is the mass loss in grams, A is the surface area in cm^2, t is the immersion time in hour, and d is the density of samples in $grams.cm^{-3}$.[39,40]

Results and Discussion

Microstructure

Figure 1 shows the general microstructure of the alloys. According to the analysis of the general microstructures, it was found that the addition of 0.5 wt. % Ca to Alloy 1 caused an increase in the phases within the eutectic region. Furthermore, the shapes of the phases transformed from being solely spherical to a combination of spherical, and needle-like forms. Furthermore, the sizes of the intermetallics increased. With the addition of Mn, it was seen that the shapes of the intermetallics did not change, but their sizes were reduced.

The ability of elements to form compounds is influenced by differences in electronegativity.[37] Since the electronegativity difference between Mg and Sn is greater, the resulting intermetallic phase is Mg_2Sn . However, because the Al content does not surpass 2%, no alloy has contained the $Mg_{17}Al_{12}$ intermetallic.[41,42] Figure 3 reveals that Alloys 1 and 3 contain only α-Mg and Mg_2Sn, while Alloy 2 exhibits a ternary phase consisting of α-Mg and Mg_2Sn as well as CaMgSn. The EDS analyses in Figure 3(e) show α-Mg, Mg_2Sn in Alloy 1 and CaMgSn phases in Alloy 2. According to Kozlov et al. , the Sn-Ca ratio in Mg-Sn-Ca alloys is of critical importance in determining phase formation. When the ratio is three, only the CaMgSn intermetallic is present in the structure, whereas when the ratio is between five and ten, both CaMgSn and Mg_2Sn coexist.[43] Due to the Sn/Ca ratio in Alloy 2 being between 5, and 10, the EDS examination revealed the presence of both CaMgSn and Mg_2Sn phases.

Experimental alloys all contain α-Mg and Mg_2Sn. In Mg–Sn alloys, the Mg_2Sn phase, which has a melting temperature of 770.5°C, is quite stable at higher temperatures than the $Mg_{17}Al_{12}$ phase, which has a melting temperature of 417°C. Therefore, the Mg_2Sn phase improves the mechanical properties. In this study, the Al ratio was determined as 2% to prevent the formation of $Mg_{17}Al_{12}$

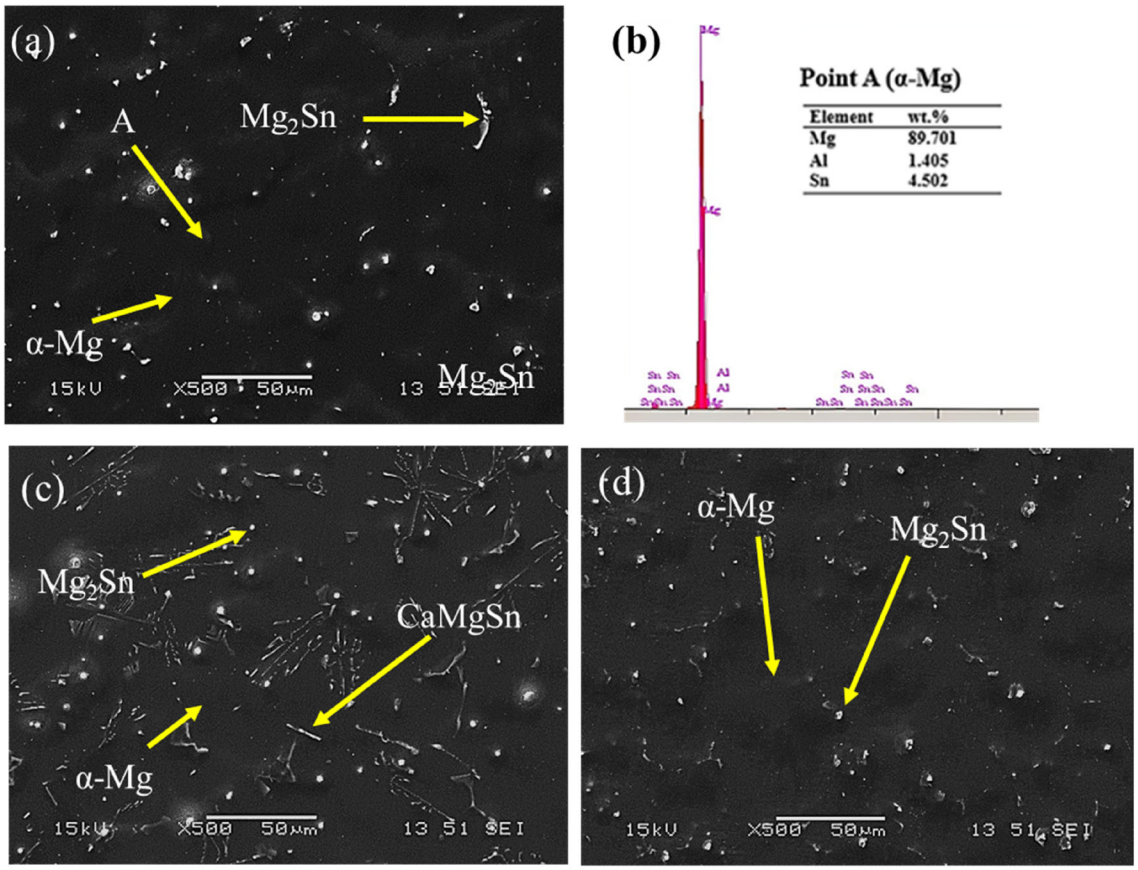

(e) Composition analysis (wt. %)

Mg	Sn	Al	Ca	Mn	Phase
93.752	3.095	1.034	-	-	α-Mg (Alloy 1)
54.187	33.810	0.611	-	-	Mg_2Sn (Alloy 1)
60.945	25.081	0.453	10.069	-	CaMgSn (Alloy 2)
92.398	3.782	1.144	-	0.707	α-Mg (Alloy 3)

Figure 4. SEM micrograph illustrating the microstructure and EDS analysis of (a,b) Alloy 1, (c) Alloy 2, (d) Alloy 3, and (e) EDS phase definitions.

thus, this phase was not observed. In addition to α-Mg, and Mg_2Sn, a triple CaMgSn phase was detected in the XRD spectrum (Figure 4) with the addition of Ca. With the addition of Mn, no new intermetallic compounds were formed as seen in the XRD spectrum. However, in the EDS results obtained from the α-Mg region for Alloy 3, Mn was detected at 0.707 wt% (Figure 3(e)). XRD results were obtained in accordance with the microstructure.

Grain refinement has been accepted as an alternative approach to overcome the problems related to Mg and its alloys.[44] This is because grain refinement can simultaneously improve strength, hardness toughness, and ductility, and reduce casting defects such as segregation and porosity. Also, Ca comes second to zirconium and shows strong potential in Mg alloys as a competitive grain refiner in Mg-Al-based alloys. Grain refinement is the restriction of grain growth, usually in an area immediately adjacent to the solid/liquid interface, due to supercooling. The distribution of eutectic phases, and solute elements along interdendritic areas and grain boundaries limits grain size.[44,45] The optical microscope images of the alloys are given in Figure 5. In Figure 5, the light coloured regions indicate α-Mg, and the dark regions indicate grain boundaries, and intermetallics located at the grain boundaries. Using the optical microscope images in Figure 5, grain size was determined by the intercept method according to ASTM standard E112-13 (2021).[46] The grain

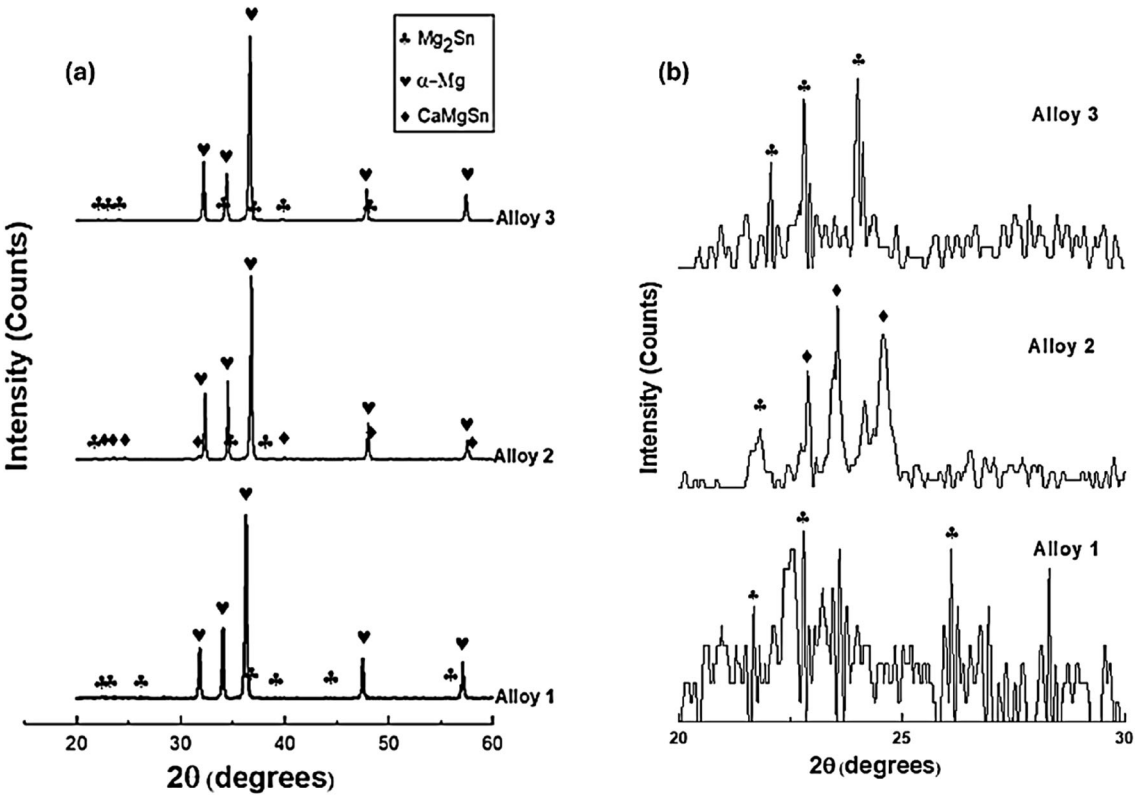

Figure 5. XRD patterns of (a) Alloys, and (b) Mg2Sn and CaMgSn peaks at 20-30 degrees.

Table 2. Mechanical Properties of Alloys

Alloy No.	$YTS_{0.2}$ (MPa)	UTS (MPa)	ε (Elongation)	n (Strain hardening exponent)	r (Anisotropy coefficient)	HB (Brinell Hardness)
Alloy 1	75 ± 4	131 ± 5	9.2 ± 0.4	0.35	0.803	30 ± 0.6
Alloy 2	45 ± 6	92.5 ± 7	7.3 ± 0.3	0.28	0.872	28.5 ± 0.5
Alloy 3	60 ± 7	102 ± 9	9.3 ± 0.5	0.36	1.293	34 ± 0.8

size for Alloy 1 was calculated as 105μm, for Alloy 2 as 90 μm, and for Alloy 3 as 60 μm. Especially with the addition of Mn, it was observed that the grains turned into equiaxed grains.

Mechanical Properties

The mechanical properties of the post-casting alloys are given in Table 2 and Figure 6. It is thought that the added alloying elements reduce the α-Mg grain size, and form intermetallics at the grain boundaries. Therefore, this will provide a solid solution for the hardening of the alloy, and increase the alloy's strength. For this purpose, the mechanical behavior of the alloys produced was investigated. The tensile strength of the master alloy was determined as 131 MPa, the yield strength was 75 MPa and the elongation was 9.2%.

The lowest yield strength, tensile strength, and elongation values were obtained with the addition of Ca. Compared to the Mg-4Sn-2Al alloy, the tensile strength value of Alloy 2 decreased by 29% to 92.5 MPa, the yield strength decreased by 40% to 45 MPa, and the elongation decreased by 20% to 7.38. It is thought that this is due to the CaMgSn phase that occurs with the addition of Ca. Despite the high thermal stability of the CaMgSn phase in the Mg-Sn-Ca alloy in the literature, its coarse morphology tends to separate due to the stress concentration of dendritic intermetallics along grain boundaries during the loading process.[47,48] Therefore, dendritic intermetallics are known to cause brittle intergranular cracking. Coarse, and continuous intermetallics are thought to impair strength and ductility. Li et al. investigated the mechanical properties of Mg-2Zn alloy with 0.2, 0.4, and 0.8 Ca added.[49] The mechanical properties were improved by the addition of 0.2 Ca. However, when the amount of Ca increased, the mechanical properties were adversely affected. With the addition

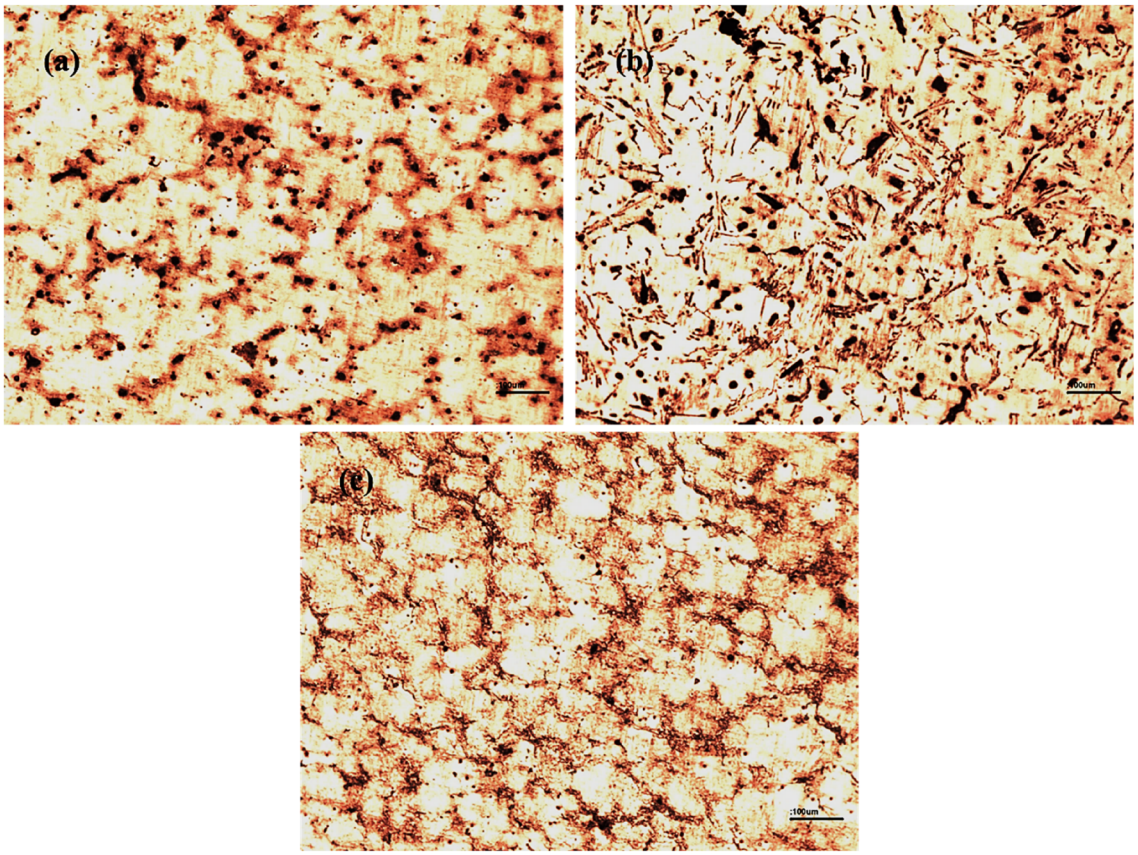

Figure 6. Optical Microscope images of (a) Alloy 1, (b) Alloy 2, and (c) Alloy 3.

of Mn, the yield strength and tensile strength of Alloy 1 decreased, while the elongation, and strain hardening exponent values remained approximately the same. This is because Mn does not have much effect on tensile strength, as stated in the literature.[50] In addition, according to the EDS results (Figure 7) obtained from the regions close to the grain boundaries of the alloys, Alloy 1 contains 2 wt.% Al and 4 wt.% Sn. With the addition of Ca, these values decreased to 0.45 Al and 1.94 Sn. Similarly, with the addition of Mn, the values changed to 1 Al and 3.7 Sn. These results show that the dissolution of Al and Sn atoms in the α-Mg region (solid solution hardening) is higher in Alloy 1. Solid solution hardening is less effective in alloys with Ca and Mn additions than in Alloy 1. Therefore, the yield strength and tensile strength of Alloy 1 are higher. Although the grain size decreased with the addition of alloying elements, mechanical properties did not improve. Additionally, Pan et al. reported that the large eutectic phases (CaMgSn) distributed between the dendritic gaps due to the slow cooling rate of the Mg–2Sn–1Ca alloy during casting caused the yield strength value to decrease.[51]

Based on the analysis, it has been concluded that the *n* values of Alloy 2, and Alloy 3 are in line with the elongation outcomes. Additionally, it has been observed that the plastic deformation capability decreases with the inclusion of Ca, while it stays unchanged with the inclusion of Mn. It is thought that with the addition of Ca to Alloy 1, the CaMgSn intermetallic seen in the microstructure may have functioned as crack initiation sites. Thus, the formability was negatively affected, and the *n* value decreased. With the addition of Mn, the hardening exponent remained almost the same. Liao et al. showed that when 1 wt% Mn was added to the extruded Mg-1Sn alloy, the hardening exponent decreased from 0.19 to 0.14.[52] Grain refinement, and the distribution of grain orientation were expressed as the cause of the strain hardening exponent decreasing. In addition, Zhao et al. stated that grain refinement may result in a slower dislocation storage rate, and less twinning, and then the increase in strain hardening can be limited.[53]

A common method of evaluating anisotropy in a sheet material is to calculate the ratio between strains across the width and thickness, called the anisotropy coefficient. The anisotropic properties of a material depend on both alloy composition, and processing history. Anisotropic properties can significantly impact sheet-forming processes, particularly deep drawing, and stretch forming. Therefore, the anisotropy coefficient is considered an important parameter for characterizing a metal plate's ability to sustain deformation.[54] The anisotropy coefficient was obtained by the ratio of the true transverse strain value ε_w to the actual strain value ε_t in thickness, as stated in Equation 2.

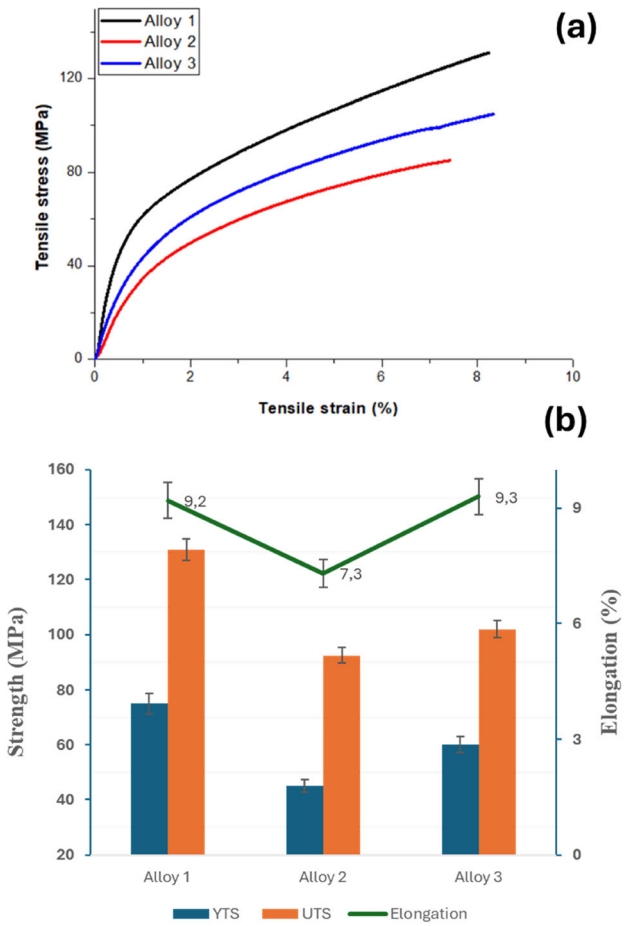

Figure 7. Mechanical properties of alloy (a) Tensile strain–Tensile stress, (b) UTS and Elongation.

Considering the incompressibility of the material, the equation $\varepsilon_w + \varepsilon_t + \varepsilon_l = 0$ is valid. The sum of the plastic deformations in the material's width, length, and thickness directions is zero. For Alloy 1 and Alloy 2, r <1 was determined. Because the change in thickness is greater than the change in width. The anisotropy coefficient for Alloy 3 was found to be 1.293, and since this value is greater than 1 (r>1), it can be said that the variation in the width of the alloy is greater. The anisotropy coefficient affects the deep drawability and formability of the material. According to the results obtained, Alloy 3 has the highest anisotropy coefficient and can be shaped better than other alloys since r>1.[55] Elsayed et al. investigated the anisotropic behavior of hot extruded powder metallurgy Mg–Al–Mn–Ca and Mg–Al–Zn–Ca–La alloys under both tensile, and compressive loadings and compared their anisotropies. It was stated that the addition of La showed a remarkable improvement in anisotropy.[56] In rolled Mg-Gd-Zn alloys, r-values close to 1 indicate that cross-sectional reduction occurs isotropically, meaning that the stresses in the width and thickness directions are comparable. It is well established that r-values are strongly correlated with crystallographic texture. Rolled Mg-Gd-Zn alloys exhibit a relatively random texture, with most grains favorably oriented for basal slip during tensile testing. This favorable orientation facilitates the generation of comparable stresses in the thickness, and width directions. Consequently, a moderate r-value close to 1 is achieved, reflecting the isotropic nature of the deformation.[57]

The tensile test findings show that the elongation of Alloy 2 is reduced compared to Alloy 1, whereas the elongation of Alloy 3 remains essentially unchanged. Examination of fracture surfaces similarly shows the same result. Fracture surfaces of Mg-4Sn-2Al, Mg-4Sn-2Al-0.5Ca, and Mg-4Sn-2Al-0.25Mn alloys are shown in Figure 8. The presence of large cleavage planes on the fracture surface of the Mg-4Sn-2Al-0.5Ca alloy in Figure 8b suggests that it undergoes less plastic deformation. In other respects, it can be stated that Alloy 1, and Alloy 3 undergo more plastic deformation than Alloy 2, since the cleavage planes on the fracture surfaces are narrower than Alloy 2, and the number, and width of dimples are greater.

Corrosion Behavior

Many factors such as impurities, secondary phases, surface films, and grain boundaries affect the corrosion behavior of Mg alloys. However, the corrosion resistance of Mg alloys is mainly related to two factors, which are the properties of the surface film, and the amount of electrochemically inert secondary phase particles or impurities. Unlike Al alloys, the surface film of Mg is not protective, which causes poorer corrosion resistance of Mg alloys. In addition, in Mg alloys, almost all intermetallics or impurities are nobler than the matrix. Therefore, micro-galvanic corrosion occurs between intermetallics, and α-Mg. Accordingly, it is very important to control the microstructure, especially the formation of intermetallics, and to form a stable, and protective film in order to improve the corrosion resistance of Mg Alloys.[58]

The potentiodynamic polarization curves of the alloys are given in Figure 9. The Tafel extrapolation method was used to determine the corrosion current from the polarization curves. The Tafel extrapolation method is used to determine the corrosion current (I_{corr}), corrosion potential (E_{corr}), and corrosion rate in an electrochemical cell. The current produced in an electrochemical cell when corrosion occurs is the corrosion current. While the corrosion current is 90.69 μA for Alloy 1, this value is 127.1 μA for Alloy 2, and 37.33 μA for Alloy 3. As can be seen in Equation 3, the corrosion rate is directly proportional to the corrosion current. With the addition of Ca, the corrosion current increased, and the corrosion rate increased accordingly. In the literature, it has been stated that the coarse triple CaMgSn phase that appears in the microstructure separates from the matrix, and damages the passive film.[59] It has been reported that elongated mesh cracks can be observed

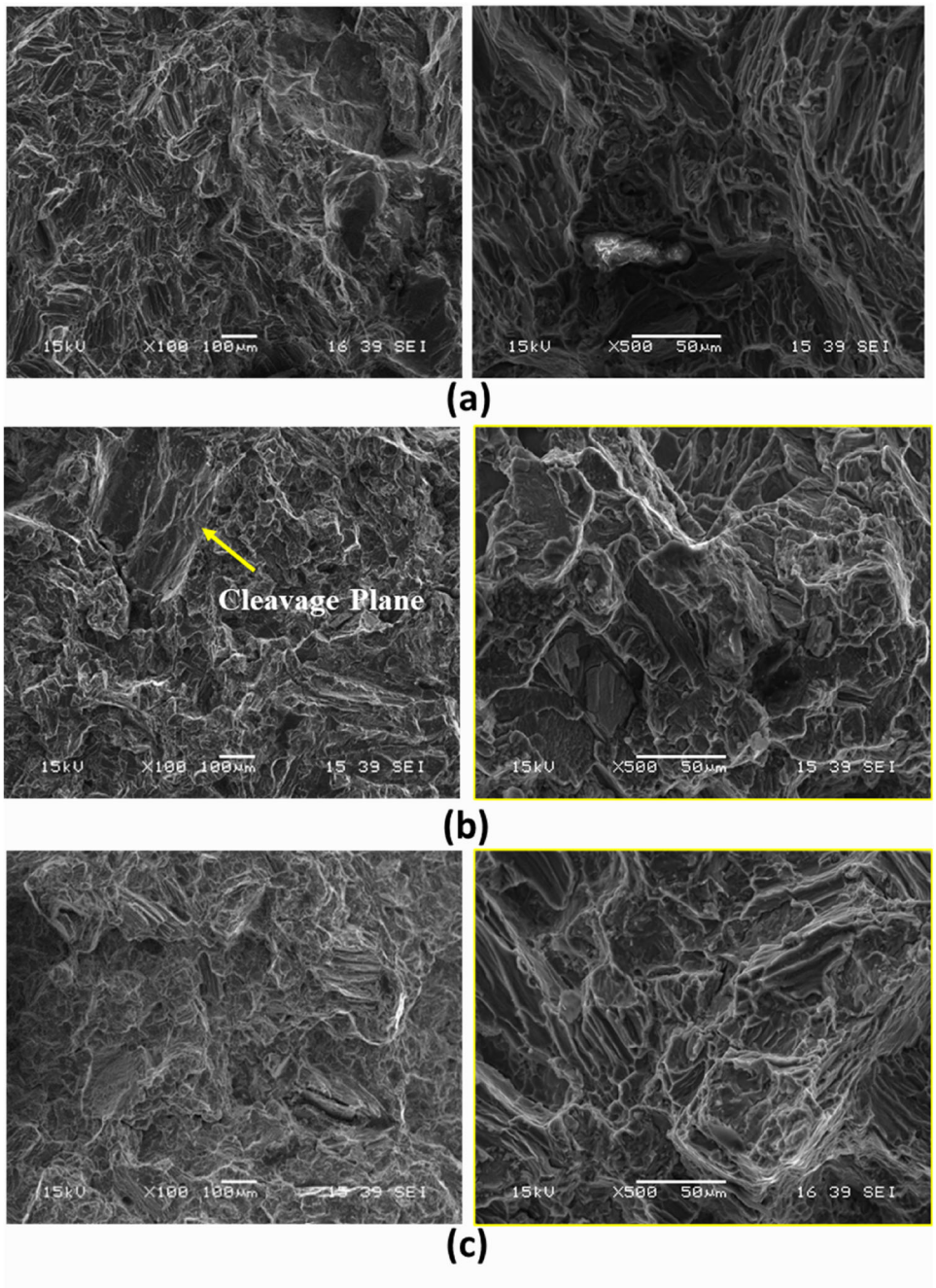

Figure 8. SEM images of fracture surfaces at room temperature for (a) Alloy 1, (b) Alloy 2, and (c) Alloy 3.

in the passive film and reduce the corrosion resistance of the alloys.

The addition of Mn increased the corrosion resistance of the alloy, and reduced the corrosion rate to 18.96 mpy. The reason for this is that the grain size decreases with the addition of Mn, causing the Mg_2Sn phase at the grain boundaries to be more spherical, and smaller in size. Therefore, it is thought that Mg_2Sn, which acts as a cathode in micro-galvanic corrosion, may have corroded its surroundings. Li et al. investigated the corrosion properties of Mg-10Al alloy by adding 0.3, 0.6, 0.9, and 1.2 Mn wt. %.[60] According to the results obtained, the addition of 0.6 Mn showed the best corrosion resistance. It was stated that the addition of Mn resulted in a new phase emerging in the microstructure. When the Mn ratio was 0.9, and 1.2, it was stated that the micro-galvanic corrosion increased because the amount of the phase increased. Some suggested that the presence of Mn in the alloy increased the corrosion rate compared to when there was no Mn added.

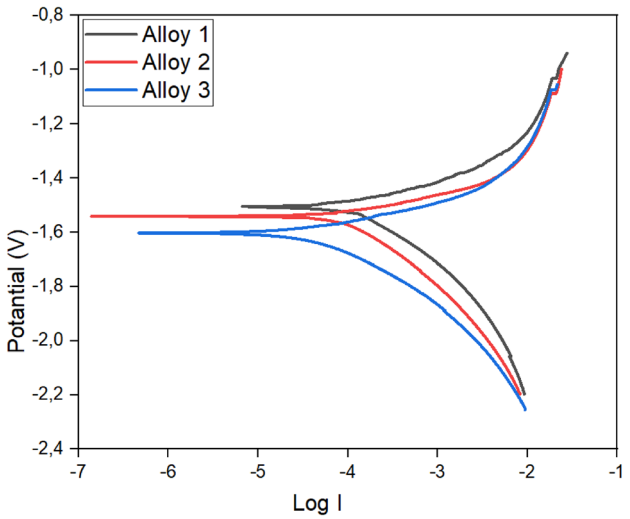

Figure 9. Potentiodynamic polarization curves of alloys.

Table 3. Potentiodynamic Polarization Results of Alloys

Alloy No.	E_{corr} (V)	I_{corr}(μA)	R_{corr}(mpy)	R_w(mpy)
Alloy 1	− 1.483	90.69	46.60	932.46
Alloy 2	− 1.542	127.1	66.19	528.92
Alloy 3	− 1.603	37.33	18.96	65.32

The E_{corr}, I_{corr}, and R_{corr} values obtained from the polarization curves of each three alloys are summarized in Table 3.

SEM micrographs, and regional EDS analyses of the surfaces of the corroded alloys are given in Figure 10. When the corrosion surfaces of the alloys are examined, it is seen that the Mg_2Sn intermetallic phase in all three alloys settles at the grain boundaries. This leads to the formation of the micro-galvanic cell of Mg_2Sn/α-Mg, which corrodes the α-Mg matrix, which acts as the anode, and intergranular corrosion occurs. Micro-galvanic cells are formed where intermetallic phases occur, and act as cathodes of micro-galvanic cells, they do not corrode themselves, but cause corrosion of their surroundings, which act as anodes. Therefore, the cathode/anode area ratio is very important in galvanic corrosion. The smaller the anode area, the greater the anode current density, and the faster the anode will corrode. Therefore, as the size of the intermetallics decreases, the corrosion rate will decrease. The increase in the size, and amount of CaMgSn intermetallic with the addition of Ca caused an increase in the corrosion rate. Hort et al. examined the effects of Ca addition to Mg-Sn alloys on corrosion resistance, and when they evaluated the results, they clearly showed the detrimental role of calcium, revealing that tin, and calcium have opposite effects when it comes to corrosion.[61] In the same study, it was seen that Mg-6Sn-2Ca exhibited excellent corrosion resistance, but the same amount of Ca in Mg-3Sn-2Ca showed poor corrosion resistance. Therefore, they concluded that the relative amounts of Ca, and Sn should also be considered, rather than the individual amounts of the elements. The addition of Mn is thought to cause an increase in corrosion resistance by reducing the size of the Mg_2Sn intermetallic. Cho et al. reported that the addition of 0.4 wt.% Mn to the Mg-4Zn-0.5Ca alloy reduced the corrosion current of the alloy by half and the corrosion rate decreased accordingly.[62] They stated that the main reason for this was the improved stability of the MnO and MnO_2 surface corrosion product films formed on the surface by the addition of Mn. Nam showed that with the addition of 1wt.% Mn to Mg-5Al alloy, the corrosion current density (i_{corr}) decreased from 371 μA/cm^2 to 84 μA/cm^2. The corrosion resistance mechanism was attributed to the interaction of alloying element oxides with Mg and Al oxides, which act as a corrosion barrier to inhibit the corrosion process.[35]

In Table 3, both potentiodynamic, and immersion test corrosion rates of the alloys are given in mpy. It is seen that the immersion corrosion rates are higher than the potentiodynamic corrosion rates. This is because the surface areas in contact with the solution in corrosion tests are quite large in the immersion test.[63] In electrochemical corrosion, a very small area (1.77 cm^2) remained in contact with the solution. This caused the corrosion to turn into general corrosion, and the corrosion rates of the alloys were calculated to be higher.

Figure 11 shows SEM images of the corroded surfaces of the alloys after the immersion test. Alloy 3 corroded less due to its small grain size, and the size of intermetallics (Figure 11c). However, Alloy 2 with Ca addition had the highest corrosion rate according to the potentiodynamic test results, while the corrosion resistance in the immersion test was found to be higher than Alloy 1. In the EDS analyses given in Table 4, the wt.% values of O (oxygen), chlorine (CI), and Mg on corroded surfaces were compared. According to these results, the amount of chlorine in Alloy 2 is less than that in Alloy 1. Thirumalaikumarasamy et al. reported that chloride ion concentrations in magnesium alloys are closely related to the corrosion rate. They stated that the corrosion rate also increases with increasing chloride ion concentration.[63]

Electrochemical impedance spectroscopy (EIS) results were used to evaluate the electrochemical properties of the alloys. According to the results, the addition of Ca and Mn to Mg-4Sn-2Al alloy did not affect the corrosion mechanism but significantly changed the impedance values. The bode magnitude plots are seen in Figure 12(a). At low frequencies, the impedance magnitude is controlled by the charge transfer resistance (R_c) and diffusion processes of the system, while at high frequencies, the solution resistance (R_s) becomes dominant. The change of phase angle with frequency is shown in Figure 12(b). The maximum phase angle indicates the frequency at which the capacitive behavior of the system is

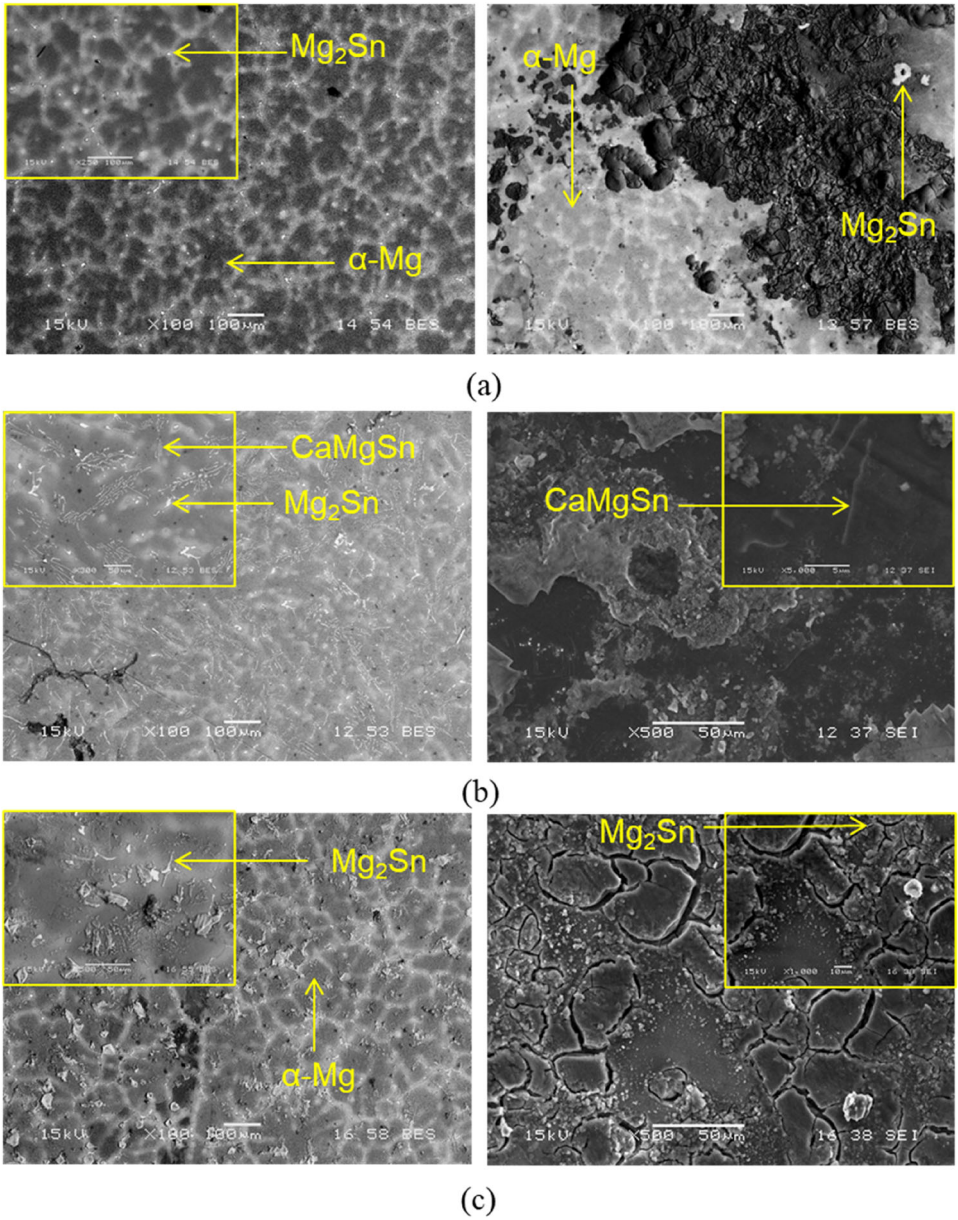

Figure 10. Electrochemical corrosion morphologies of (a) Alloy 1, (b) Alloy 2, and (c) Alloy 3.

dominant and provides information about the formation of the protective surface film. A higher maximum phase angle indicates higher corrosion resistance. The Nyquist plots for all alloys consist of only a single half-arc, indicating that a charge-controlled dissolution takes place. The diameters of the circles in the Nyquist diagrams in Figure 12(c) provide important information about the corrosion resistance of the alloys. Larger diameter circles indicate higher corrosion resistance.[58] The larger circles in Mg-4Sn-2Al-0.5Ca and Mg-4Sn-2Al-0.25Mn alloys indicate that these additives reduce corrosion by forming a protective layer on the surface. In Figure 12(d), the equivalent circuit model is used to analyze the measured EIS data. The Randal's circuit shows high compatibility with impedance results. Detailed information about the circuit can be found elsewhere.[64,65] Magnesium alloys have a passive layer based on $MgO/Mg(OH)_2$ on the surface. This layer is porous and the ions in the corrosive environment contact the base metal surface through these pores. According to the EIS test results, the addition of Mn to the Mg-4Sn-2Al alloy increased the protection of the passive layer. Microscopic, elemental and electrochemical tests will then be carried out to investigate the causes in detail.

Conclusions

Microstructural, mechanical, and corrosion properties of the alloys were investigated by the addition of Ca and Mn to the cast Mg-4Sn-2Al alloy. The results are as follows:

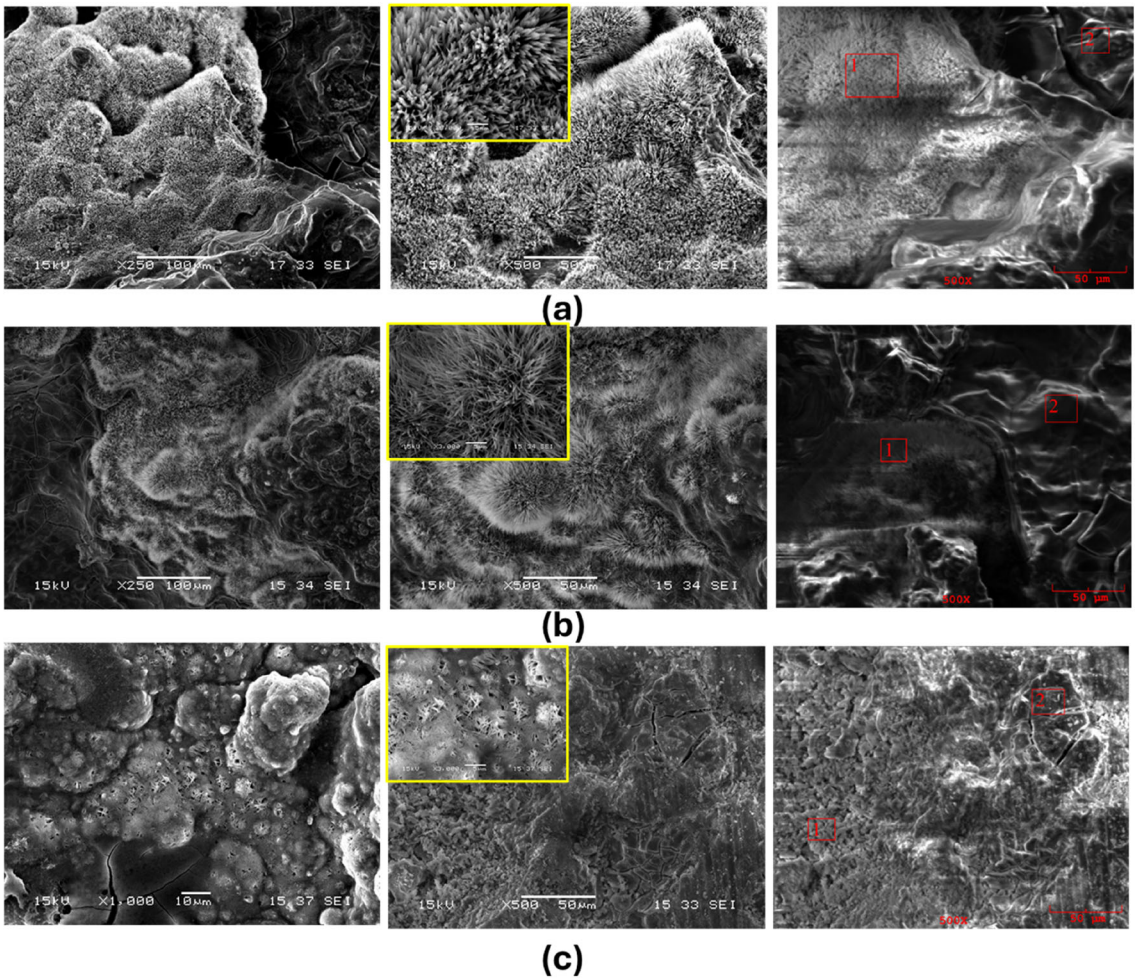

Figure 11. SEM images of corroded surfaces after immersion testing (a) Alloy 1, (b) Alloy 2, and (c) Alloy 3.

Table 4. Immersion Test EDS Results of Alloys

Alloy No.	1	2
Alloy 1		
O	40.991	49.643
Mg	37.378	50.258
Cl	21.631	0.100
Alloy 2		
O	46.603	48.297
Mg	46.716	51.549
Cl	6.681	0.154
Alloy 3		
O	42.552	48.335
Mg	53.860	49.973
Cl	–	–

1. Alloy 1's microstructure consists of α-Mg and Mg_2Sn phases. The addition of Ca resulted in the formation of a needle-like CaMgSn intermetallic structure. While the addition of Mn did not create a new phase in the microstructure, it led to the reduction in size, and sphericalization of the Mg_2Sn intermetallic. Additionally, the addition of both alloying elements contributed to the decrease in grain size.
2. Yield strength and tensile strength values decreased with the addition of Ca, and Mn. The lower solubilities of Al and Sn in the grain boundary regions with the addition of Ca and Mn compared to the Mg-4Sn-2Al alloy caused a decrease in yield strength and tensile strength values. Grain size, shape and size of intermetallics were effective on hardness results. It is thought that the intense load of the tip penetrating the sample in the measurement does not increase the hardness by causing fracture of the intermetallics. It is seen that especially the large size phase (CaMgSn) does not improve the

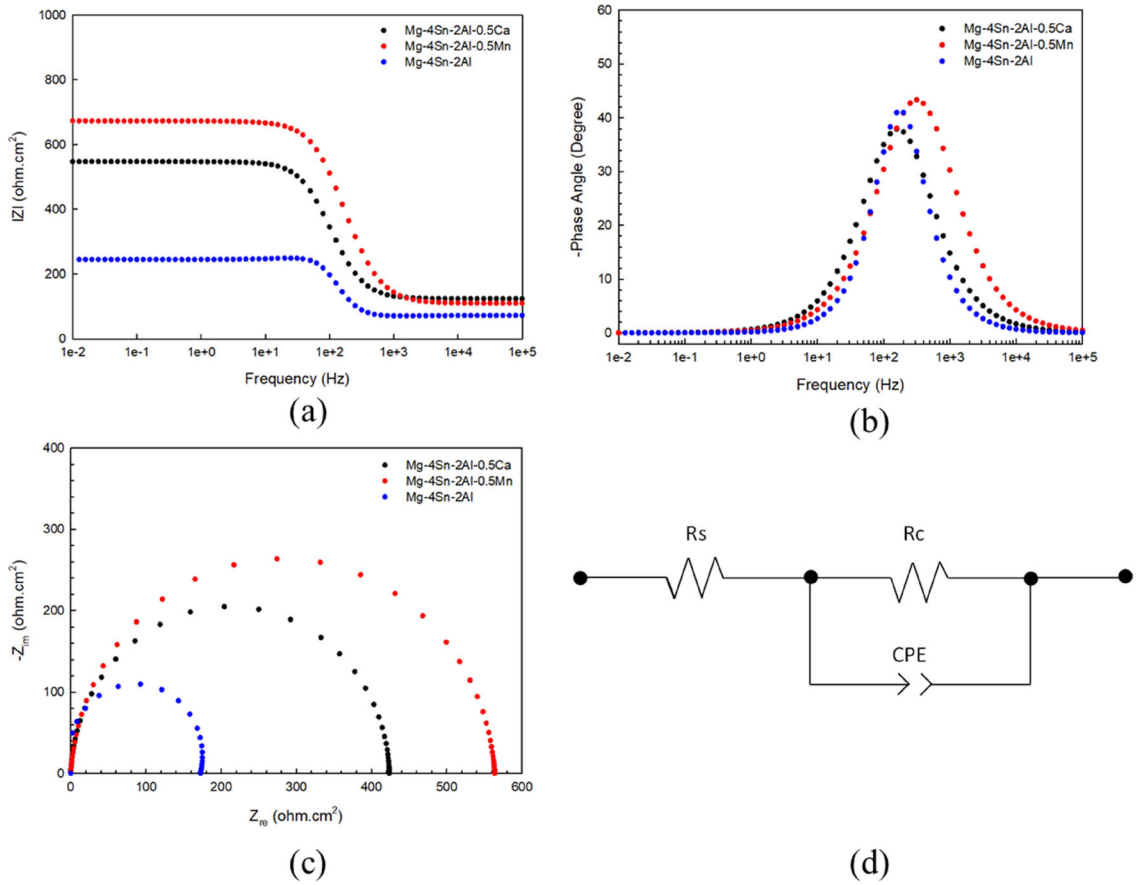

Figure 12. (a) Bode plots of impedance vs. frequency, (b) Bode plots of phase angle vs. frequency, (c) Nyquist plots of the alloys, and (d) equivalent circuit used to fit the EIS spectra.

Brinell hardness. The anisotropy coefficient increased with the addition of Mn. It has been understood that the Mn-doped alloy is more resistant to deformation in the thickness direction.

3. According to the potentiodynamic test results, Alloy 3 has the lowest corrosion rate of 18.96 mpy, indicating the highest corrosion resistance. Alloy 2 has the highest corrosion rate of 66.19 mpy, indicating the lowest corrosion resistance. The corrosion resistance of Alloy 1 increased with the addition of Mn. The reason for this is thought to be that the Mg_2Sn phase becomes smaller, and more spherical in size with the addition of Mn. It is thought that Mg_2Sn may have caused less corrosion by acting as a cathode in micro-galvanic corrosion with the reduction of its dimensions. The addition of Ca adversely affected the corrosion properties, and increased the corrosion rate. It is thought that the high amount of coarse CaMgSn intermetallic may have increased the number of galvanic cells, and decreased the corrosion resistance of the alloy.
4. According to the immersion test, Alloy 3 has the lowest corrosion rate value with 65.32 mpy, indicating that this alloy has the least material loss from the surface. Alloy 1 has the highest corrosion rate value with 932.46 mpy and it can be said that there is more material loss on the surface than other alloys.
5. Potentiodynamic corrosion rates and immersion corrosion rates of the alloys differed. The corrosion rates obtained from the immersion test results are high. This is thought to be due to the different surface areas of the test specimens. Larger surface areas in the immersion test caused the alloys to corrode more.
6. The maximum phase angle and Nyquist plots demonstrate that the addition of Ca and Mn enhances corrosion resistance by promoting the formation of a protective surface layer.

Funding

Open access funding provided by the Scientific and Technological Research Council of Türkiye (TÜBITAK).

REFERENCES

1. W. Lei, D. Zhu, H. Wang, W. Liang, Microstructure and Mechanical Properties of Pure Magnesium Subjected to Hot Extrusion. J. Wuhan Univ. Technol. Mater. Sci. Ed. **34**(5), 1193–1196 (2019). https://doi.org/10.1007/s11595-019-2177-9
2. J. Ma, Q. Wei, T. Le, J. Wang, and P. Jin, "Effect of Sn addition on the microstructure and mechanical properties of AZ31 alloys," Mater. Res. Express, vol. 7, no. 12, 2020, https://doi.org/10.1088/2053-1591/abcda8.
3. Q. Xie, A. Ma, J. Jiang, Z. Cheng, D. Song et al., "Stress corrosion cracking behavior of fine-grained AZ61 magnesium alloys processed by equal-channel angular pressing," Metals (Basel)., vol. 7, no. 9, 2017, https://doi.org/10.3390/met7090343.
4. B. Wang, F. Pan, X. Chen, W. Guo, J. Mao, Microstructure and mechanical properties of as-extruded and as-aged Mg-Zn-Al-Sn alloys. Mater. Sci. Eng. A **656**, 165–173 (2016). https://doi.org/10.1016/j.msea.2016.01.002
5. H.Y. Wang, X.L. Nan, N. Zhang, C. Wang, J.G. Wang, Q.C. Jiang, Strong strain hardening ability in an as-cast Mg-3Al-3Sn alloy. Mater. Chem. Phys. **132**(2–3), 248–252 (2012). https://doi.org/10.1016/j.matchemphys.2011.12.036
6. Y. Gu, F. Wang, J. Jiao, Z. Wang, L. Zhao, P. Mao et al. "Study on Semisolid Rheo-Diecasting Process, Microstructure and Mechanical Properties of Mg-6Al-1Ca-0.5Sb Alloy with High Solid Fraction," Int. J. Met., 2023, https://doi.org/10.1007/s40962-023-01001-0.
7. T. Li, F. Wang, X. Du, S. Bai, W. Wang, Z. Wang et al., Research Status and Prospect of Hot Tearing of Mg–Al Alloys. Int. J. Met. (2023). https://doi.org/10.1007/s40962-023-00981-3
8. I. Yıldız, Tribological properties and characterization of borided Co-Mg alloys. Open Chem. **20**(1), 277–286 (2022). https://doi.org/10.1515/chem-2022-0133
9. G. Nayyeri, R. Mahmudi, The microstructure and impression creep behavior of cast, Mg–5Sn–xCa alloys. Mater. Sci. Eng. A **527**(7), 2087–2098 (2010). https://doi.org/10.1016/j.msea.2009.11.053
10. E. Ghio, E. Cerri, Corrosion Behaviour of High-Pressure Die-Cast AZ91 Alloy in NaCl Solution: Effects of Friction Stir Process at High Rotational Speed. Materials **16**, 6620 (2023). https://doi.org/10.3390/ma16206620
11. P. Kumar, A. K. Bhargava, Y. V. S. S. Prasad, Govind, "Effect of Tin Additions on Microstructure and Mechanical Properties of Sand Casting of AZ92 Magnesium Base Alloy,"Mat. Sci. Res. India, vol. 10 (2), 2013,https://doi.org/10.13005/msri/100205.
12. B. Cicek, L. Elen, E. Koc, A. N. Saud, and Y. Sun, "Investigation of Intermetallic Phase Fractions and Dry-corrosive Wear Properties in Mg–Al–Si Ternary Alloy," Int. J. Met., pp. 26–28, 2023, https://doi.org/10.1007/s40962-023-00992-0.
13. Y. Meng, Y. Yang, L. Cao, J. Sun, J. Cui, Effect of Al Content on the Solidification Behaviors of Mg–Al Alloys. Int. J. Met. **17**, 703–716 (2023). https://doi.org/10.1007/s40962-022-00798-6
14. R. Mahmudi, F. Kabirian, Z. Nematollahi, Microstructural stability and high-temperature mechanical properties of AZ91 and AZ91+2RE magnesium alloys. Mater. Des. **32**(5), 2583–2589 (2011). https://doi.org/10.1016/j.matdes.2011.01.040
15. B.H. Kim, H. Kimura, Y.H. Park, I.M. Park, The effect of cerium on microstructures and mechanical properties of Mg-4A1-2Sn-1Ca Alloy. Mater. Trans. **51**(7), 1346–1349 (2010). https://doi.org/10.2320/matertrans.M2010042
16. F.R. Elsayed, T.T. Sasaki, C.L. Mendis, T. Ohkubo, K. Hono, Compositional optimization of Mg-Sn-Al alloys for higher age hardening response. Mater. Sci. Eng. A **566**, 22–29 (2013). https://doi.org/10.1016/j.msea.2012.12.041
17. D.H. Kim, H.K. Lim, Y.K. Kim, J.S. Kyeong, W.T. Kim, D.H. Kim, High temperature deformation behavior of Mg-Sn(-Zn) alloy. Met. Mater. Int. **17**(3), 383–388 (2011). https://doi.org/10.1007/s12540-011-0003-9
18. K.C. Park, B.H. Kim, J.J. Jeon, Y.H. Park, I.M. Park, The influence of Sn addition on the corrosion behavior of Mg-5Al-1Zn alloy. Mater. Sci. Forum **620**(622), 153–156 (2009). https://doi.org/10.4028/www.scientific.net/MSF.620-622.153
19. Y. Turen, Effect of Sn addition on microstructure, mechanical and casting properties of AZ91 alloy. Mater. Des. **49**, 1009–1015 (2013). https://doi.org/10.1016/j.matdes.2013.02.037
20. S.H. Park, J.G. Jung, J. Yoon, B.S. You, Influence of Sn addition on the microstructure and mechanical properties of extruded Mg-8Al-2Zn alloy. Mater. Sci. Eng. A **626**, 128–135 (2015). https://doi.org/10.1016/j.msea.2014.12.039

21. N. Hort, Y. Huang, T.A. Leil, P. Maier, K.U. Kainer, Microstructural investigations of the Mg-Sn-xCa system. Adv. Eng. Mater. **8**(5), 359–364 (2006). https://doi.org/10.1002/adem.200600014
22. H. Liu, Y. Chen, Y. Tang, S. Wei, G. Niu, The microstructure, tensile properties, and creep behavior of as-cast Mg-(1–10)%Sn alloys. J. Alloys Compd. **440**(1–2), 122–126 (2007). https://doi.org/10.1016/j.jallcom.2006.09.024
23. J.S. Zhang, Y. Sun, W.L. Cheng, Z.P. Que, Y.M. Li, L. Liushan, "The effect of Ca addition on microstructures and mechanical properties of Mg-RE based alloys," J. Alloys Compd., vol. 554, pp. 110–114, 2013, https:// doi.org/https://doi.org/10.1016/j.jallcom.2012.11.094.
24. S. Acikgoz, S.C. Kurnaz, The Effects of Individual Addition of Sn, Nd, and Ca on the Microstructure, Mechanical Properties, and Corrosion Behavior of the Mg–Li–Al Alloy. Int. J. Met. (2022). https://doi.org/10.1007/s40962-022-00869-8
25. J. Bao, J. Sha, L. Li, Z. Liu, J. Tian, W. Liu et al., Electrochemical properties and discharge performance of Mg-3Sn-xCa alloy as a novel anode for Mg-air battery. J. Alloys Compd. **934**, 167849 (2023). https://doi.org/10.1016/j.jallcom.2022.167849
26. K. Suresh, K.P. Rao, Y.V.R.K Prasad, N. Hort, K.U Kainer, "Microstructure and mechanical properties of as-cast Mg-Sn-Ca alloys and effect of alloying elements," Trans Nonferrous Met. Soc. China, 2013;23(12):3604–10.https://doi.org/10.1016/S1003-6326(13)62907-6.
27. G. Nayyeri, R. Mahmudi, Effects of Ca additions on the microstructural stability and mechanical properties of Mg-5%Sn alloy. Mater. Des. **32**(3), 1571–1576 (2011). https://doi.org/10.1016/j.matdes.2010.09.019
28. P. Hua, H. Zou, Y. Chai, X. Chen, H. Yang, Y. Zhang et al., The effect of various Sn and Ca equal proportional addition on the microstructure, mechanical behavior and corrosion performance of Mg alloys. Mater Today Commun. **41**(July), 110466 (2024). https://doi.org/10.1016/j.mtcomm.2024.110466
29. X. Song, Y. Hu, J. Tian, Y. Wang, Z. Yan, "Effects of Addition of Yttrium on the Microstructure, Compression Properties and Corrosion Resistance of Injection Molding AZ91D-1.6Ca Magnesium Alloy," Int. J. Met., 2023, https://doi.org/10.1007/s40962-023-00997-9.
30. J. Wang, R. Lu, D. Qin, X. Huang, F. Pan, A study of the ultrahigh damping capacities in Mg-Mn alloys. Mater. Sci. Eng. A **560**, 667–671 (2013). https://doi.org/10.1016/j.msea.2012.10.010
31. M.X. Zhang, P.M. Kelly, Edge-to-edge matching and its applications: Part II. Application to Mg-Al, Mg-Y and Mg-Mn alloys. Acta Mater. **53**(4), 1085–1096 (2005). https://doi.org/10.1016/j.actamat.2004.11.005
32. J.D. Robson, D.T. Henry, B. Davis, Particle effects on recrystallization in magnesium-manganese alloys: Particle pinning. Mater. Sci. Eng. A **528**(12), 4239–4247 (2011). https://doi.org/10.1016/j.msea.2011.02.030
33. S. Aravindan, P.V. Rao, K. Ponappa, Evaluation of physical and mechanical properties of AZ91D/SiC composites by two step stir casting process. J. Magnes Alloy **3**(1), 52–62 (2015). https://doi.org/10.1016/j.jma.2014.12.008
34. C. Hou, Z. Ye, F. Qı, Q. Wang, L. Lı, X. Ouyang et al., "Effect of Al addition on microstructure and mechanical properties of Mg−Zn−Sn−Mn alloy," Trans. Nonferrous Met. Soc. China, English Ed., vol. 31, no. 7, pp. 1951–1968, 2021, https://doi.org/10.1016/S1003-6326(21)65629-7.
35. N.D. Nam, Corrosion behavior of Mg-5Al based magnesium alloy with 1 wt.% Sn, Mn and Zn additions in 3.5 wt.% NaCl solution. J. Magnes. Alloy. **2**(2), 190–195 (2014). https://doi.org/10.1016/j.jma.2014.06.002
36. H. Zengin, Role of Sr in Microstructure, Hardness and Biodegradable Behavior of Cast Mg–2Zn–2Ca–0.5Mn (ZXM220) Alloy for Potential Implant Application. Int. J. Met. **14**, 442–453 (2020). https://doi.org/10.1007/s40962-019-00366-5
37. P. Kurt, S.C. Kurnaz, Investigation of the Effect of La and Ti Addition to Mg–4Sn–2Al Alloy on Microstructure, Mechanical and Corrosion Properties. Int. J. Met. **17**, 1388–1401 (2023). https://doi.org/10.1007/s40962-022-00875-w
38. E. Kocaman, B. Kılınç, M. Durmaz, Ş Şen, U. Şen, The influence of chromium content on wear and corrosion behavior of surface alloyed steel with Fe(16–x)Crx(B, C)4 electrode. Eng. Sci. Technol. an Int. J. **24**(2), 533–542 (2021). https://doi.org/10.1016/j.jestch.2020.08.003
39. Astm International, "G31-72: Standard Practice for Laboratory Immersion Corrosion Testing of Metals," An Am. Natl. Stand., vol. 03.02, no. Reapproved, pp. 1–8, 2012. https://www.astm.org/standards/g31.
40. H. Zengin, Y. Turen, H. Ahlatcı, Y. Sun, and A. C. Karaoğlanlı, "Influence of Sn addition on microstructure and corrosion resistance of AS21 magnesium alloy," Trans. Nonferrous Met. Soc. China (English Ed., vol. 29, no. 7, pp. 1413–1423, 2019, https://doi.org/10.1016/S1003-6326(19)65048-X.
41. F. Habashi, "Alloys: Preparation, Properties, Applications," Isbn 3-527-29591-7, Wıley-Vch Verlag Gmbh, D-69469 Weinheim, Germany, 321,1998.
42. Q. Wang, Y. Chen, S. Xiao, X. Zhang, Y. Tang, S. Wei et al., Study on microstructure and mechanical properties of as-cast Mg–Sn–Nd Alloys. J. Rare Earths **28**(5), 790–793 (2010). https://doi.org/10.1016/S1002-0721(09)60202-7
43. A. Kozlov, M. Ohno, T.A. Leil, N. Hort, K.U. Kainer, R. Schmid-Fetzer, Phase equilibria, thermodynamics and solidification microstructures of Mg-Sn-Ca alloys, Part 2: Prediction of phase formation in Mg-rich Mg-Sn-Ca cast alloys. Intermetallics **16**(2), 316–321 (2008)

44. Y. Ali, D. Qiu, B. Jiang, F. Pan, M.X. Zhang, Current research progress in grain refinement of cast magnesium alloys: A review article. J. Alloys Compd. **619**, 639–651 (2015). https://doi.org/10.1016/j.jallcom.2014.09.061
45. S.E. Harandi, M. Mirshahi, S. Koleini, M.H. Idris, H. Jafari, M.R.A. Kadir, Effect of calcium content on the microstructure, hardness and in-vitro corrosion behavior of biodegradable Mg-Ca binary alloy. Mater. Res. **16**(1), 11–18 (2013). https://doi.org/10.1590/S1516-14392012005000151
46. ASTM E112-13(2021); Standard Test Methods for Determining Average Grain Size, Standard. ASTM International: West Conshohocken, PA, USA, 2021. Available online: https://www.astm.org/e0112-13r21.html (accessed on 20 April 2022).
47. B.H. Kim, H. Kimura, Y.H. Park, I.M. Park, The effect of cerium on microstructures and mechanical properties of Mg-4A1-2Sn-lCa Alloy. Mater. Trans. **51**(7), 1346–1349 (2010). https://doi.org/10.2320/matertrans.M2010042
48. M.B. Yang, Y.L. Ma, F.S. Pan, Effects of little Ce addition on as-cast microstructure and creep properties of Mg-3Sn-2Ca magnesium alloy. Trans. Nonferrous Met. Soc. China English Ed. (2009). https://doi.org/10.1016/S1003-6326(08)60411-2
49. H.X. Li, S.K. Qin, C.L. Yang, Y.Z. Ma, J. Wang, Y.J. Liu et al., Influence of Ca addition on microstructure, mechanical properties and corrosion behavior of Mg-2Zn alloy. China Foundry **15**(5), 363–371 (2018). https://doi.org/10.1007/s41230-018-7203-6
50. Z. Zhen, T. Xi, Y. Zheng, L. Li, L. Li, InVitro study on Mg-Sn-Mn Alloy as biodegradable metals. J. Mater. Sci. Technol. **30**(7), 675–685 (2014). https://doi.org/10.1016/j.jmst.2014.04.005
51. H. Pan, G. Qin, M. Xu, H. Fu, Y. Ren, F. Pan et al., Enhancing mechanical properties of Mg-Sn alloys by combining addition of Ca and Zn. Mater. Des. **83**, 736–744 (2015)
52. H. Liao, J. Lim, T. Liu, A. Tang, J. She, P. Peng et al., "Effects of Mn addition on the microstructures, mechanical properties and work-hardening of Mg-1Sn alloy," Mater. Sci. Eng. A, vol. 754, no. December 2018, pp. 778–785, 2019, https://doi.org/10.1016/j.msea.2019.02.021.
53. B.H. Kim, J.J. Jeon, K.C. Park, B.G. Park, Y.H. Park, I.M. Park, Microstructural characterisation and mechanical properties of Mg-xSn-5Al-1Zn alloys. Int. J. Cast Met. Res. **21**(1–4), 186–192 (2008). https://doi.org/10.1179/136404608X361927
54. S.H. Wu, N.N. Song, F.M.A. Pires, A.D. Santos, A.B. Rocha, R. Roberto et al., The Variation of the Lankford Coefficient in Magnesium Alloy. Iddrg **2014**(June), 181–186 (2014)
55. S. Y. Betsofen, A. A. Il'In, A. A. Ashmarin, and A. A. Shaforostov, "Influence of the deformation mechanism on the anisotropy of the mechanical properties and workability of magnesium alloys," Russ. Metall., vol. 2008, no. 3, pp. 252–258, 2008, https://doi.org/10.1134/S0036029508030129.
56. A. Elsayed, J. Umeda, K. Kondoh, The texture and anisotropy of hot extruded magnesium alloys fabricated via rapid solidification powder metallurgy. Mater. Des. **32**(8–9), 4590–4597 (2011). https://doi.org/10.1016/j.matdes.2011.03.066
57. D. Wu, R.S. Chen, E.H. Han, Excellent room-temperature ductility and formability of rolled Mg-Gd-Zn alloy sheets. J. Alloys Compd. **509**(6), 2856–2863 (2011)
58. S. K. Woo, C. Blawert, K. A. Yasakau, S. Yi, N. Scharnagl, B. C. Suh et al., "Effects of combined addition of Ca and Y on the corrosion behaviours of die-cast AZ91D magnesium alloy," Corros. Sci., vol. 166, no. March 2019, p. 108451, 2020, https://doi.org/10.1016/j.corsci.2020.108451.
59. Q. Liu, W. Cheng, H. Zhang, C. Xu, J. Zhang, The role of Ca on the microstructure and corrosion behavior of Mg-8Sn-1Al-1Zn-Ca alloys. J. Alloys Compd. **590**, 162–167 (2014). https://doi.org/10.1016/j.jallcom.2013.12.077
60. X. Li, S. Liu, and Y. Du, "Investigation on the corrosion resistance of the Mg-10Al-xMn alloys based on thermodynamic calculations," Corros. Sci., vol. 189, no. June, p. 109631, 2021, https://doi.org/10.1016/j.corsci.2021.10963.
61. N. Hort, Y.D. Huang, T.A. Leil, K.P. Rao, K.U. Kainer, Properties and processing of magnesium-tin-calcium alloys. Kov. Mater. **49**(3), 163–177 (2011). https://doi.org/10.4149/km_2011_3_163
62. D.H. Cho, B.W. Lee, J.Y. Park, K.M. Cho, I.M. Park, " Effect of Mn addition on corrosion properties of biodegradable Mg-4Zn-0.5Ca-xMn alloys," J Alloys Compd. 2017;695:1166–74. Available from: https://doi.org/10.1016/j.jallcom.2016.10.244
63. D. Thirumalaikumarasamy, K. Shanmugam, V. Balasubramanian, "Comparison of the corrosion behaviour of AZ31B magnesium alloy under immersion test and potentiodynamic polarization test in NaCl solution," J. Magnes. Alloy. 2014;2(1):36–49. Available from: https://doi.org/10.1016/j.jma.2014.01.004
64. D. Sun, G.S. Frankel, W.A. Brantley, R.H. Heshmati, W.M. Johnston, "Electrochemical impedance spectroscopy study of corrosion characteristics of palladium–silver dental alloys," J. Biomed. Mater. Res. - Part B Appl Biomater. 2021;109(11):1777–86.
65. B.L. Bayode, M.L. Teffo, T. Tayler, O.O. Ige, R. Machaka, P.A. Olubambi, " Structural, mechanical and electrochemical properties of spark plasma sintered Ti-30Ta alloys," Mater Sci Eng B. 2022;283.